Journal of *Marine Science and Engineering*

MDPI

Article

X-ray Computed Tomography as a Tool for Screening Sediment Cores: An Application to the Lagoons of the Po River Delta (Italy)

Roberto Zonta [1,*], Giorgio Fontolan [2], Daniele Cassin [1] and Janusz Dominik [1]

[1] Consiglio Nazionale delle Ricerche, Istituto di Scienze Marine (CNR-ISMAR), Arsenale Tesa 104, Castello 2737F, 30122 Venezia, Italy; d.cassin@ismar.cnr.it (D.C.); janusz.dominik@ve.ismar.cnr.it (J.D.)
[2] Dipartimento di Matematica e Geoscienze, University of Trieste, CONISMA, Via Weiss, 2, 34128 Trieste, Italy; fontolan@units.it
* Correspondence: r.zonta@ismar.cnr.it

Abstract: Lagoon sediments have heterogeneous structure and texture, contain shells and plants and are often highly bioturbated and disturbed by human activities. In such sediments, the selection of representative cores and the choice of a subsampling strategy are important but difficult. In this study, we examine the usefulness of X-ray computed tomography (CT) for inferring sediment features that will help in making optimal decisions prior to core opening (24 cores from seven lagoons). Various algorithms (intensity projections, slice thickness, axial and sagittal images, CT number profiles and volumetric region of interest) are tested to visualise low- and high-density volumes or objects and to quantify the relations between the average volumetric CT number and the bulk density of the sediment matrix. The CT number is related mainly to water content and indirectly to total nitrogen and <16-µm grain-size fraction (model R^2 = 0.94). The outliers are attributed to a weak correspondence between the fraction of sediment sampled for water content determination and the volume of sediment matrix used for CT number measurements in highly heterogeneous sediment slices. In conclusion, CT is a powerful tool for the initial screening of cores recovered from heterogeneous lagoon sediments. The adequate use of available algorithms may provide quantitative information on various sediment features, allowing the purposeful selection of cores and subsamples for further investigation.

Keywords: computed tomography; CT-number; lagoon sediment; Po delta; water content; organic carbon; bulk density; grain-size; nitrogen

check for updates

Citation: Zonta, R.; Fontolan, G.; Cassin, D.; Dominik, J. X-ray Computed Tomography as a Tool for Screening Sediment Cores: An Application to the Lagoons of the Po River Delta (Italy). *J. Mar. Sci. Eng.* **2021**, *9*, 323. https://doi.org/10.3390/jmse9030323

Academic Editor: Milva Pepi

Received: 13 February 2021
Accepted: 8 March 2021
Published: 15 March 2021

Publisher's Note: MDPI stays neutral with regard to jurisdictional claims in published maps and institutional affiliations.

Copyright: © 2021 by the authors. Licensee MDPI, Basel, Switzerland. This article is an open access article distributed under the terms and conditions of the Creative Commons Attribution (CC BY) license (https://creativecommons.org/licenses/by/4.0/).

1. Introduction

Since the early work of Orsi et al. [1], X-ray computed tomography (CT) has been increasingly used for the characterisation of marine and freshwater sediment cores. This analytical technique allows the non-destructive examination of bulk density, porosity, multiplanar visualisation of structures and 3D images of larger objects, burrows and gas bubbles, and it appears as a valuable tool for controlling core quality and identifying lithology (e.g. [2–8]).

In the CT-scan analysis, the degree of attenuation of the X-radiation through the sediment core is quantified by the CT number that expresses the density range of the material on an arbitrary scale (Hounsfield units). Tomographic images are obtained by using mathematical algorithms for image reconstruction, and specialised software has advanced applications that permit detailed 2D and 3D observations of the core (e.g. [2] and references therein).

In this work, CT-scan analysis is used as an exploratory technique in the study of 24 sediment cores collected in seven lagoons of the Po River Delta (Italy). Sediments deposited in highly dynamic lagoons are characterised by strong heterogeneity, with a

variety of sediment structures formed by materials of fluvial and marine origins, as well as authigenic components, such as shells and plants. After deposition, benthic fauna modifies the sediments by changing their geotechnical properties and erosion resistance [9]. Human activities, such as fishing and dredging, further disturb deposited sediments. Until now, lagoon sediments have not been largely studied with X-ray CT techniques. The applications include the examination of stromatolites from a hypersaline lagoon [10], the estimation of the bulk density of surface sediment in the lagoon of Venice for studies on sediment erosion [11], and the identification of sedimentary facies from the Pappas Lagoon in Greece [12]. In the present study, we explore various software algorithms for optimal observation of the structure of sediment cores prior to opening. We also examine the relations between the CT number and physical and structural properties of sediment layers, particularly the water content (W_C) of the sediment matrix, in a large number of samples from different sediment types. Finally, the relations between the CT number and other properties of sediments, such as texture and organic matter (OM) content, are considered in an attempt to evaluate the limits of the X-ray CT method for predicting sediment features prior to core subsampling and analyses.

2. Materials and Methods

2.1. Study Site and Sediment Core Sampling

Before entering the Adriatic Sea, the Po River (the largest Italian watercourse: 650 km long, 71,000 km^2 basin surface area, 1455 m^3/s mean discharge [13]) forms a delta with five main distributaries (Figure 1). Two other minor streams cross the delta (Po di Levante and Po di Volano), both former branches of the Po but currently disconnected from the main watercourse. The delta includes a dozen brackish lagoons covering 18% of the 180-km^2 deltaic area [14], which are used especially for extensive aquaculture, comprising mainly mussels and Manila clams [15]. Sediments from the seven main lagoons (from north to south in Figure 1: Caleri (CL), Marinetta-Vallona (MV), Barbamarco (BA), Canarin (CN), Bonelli (BO), Scardovari (SC) and Goro (GO)) were investigated. In the spring of 2016, 24 sediment cores (35.7–59.3 cm long) in Plexiglas cylinders (internal diameter = 6.4 cm) were collected using a piston corer [16].

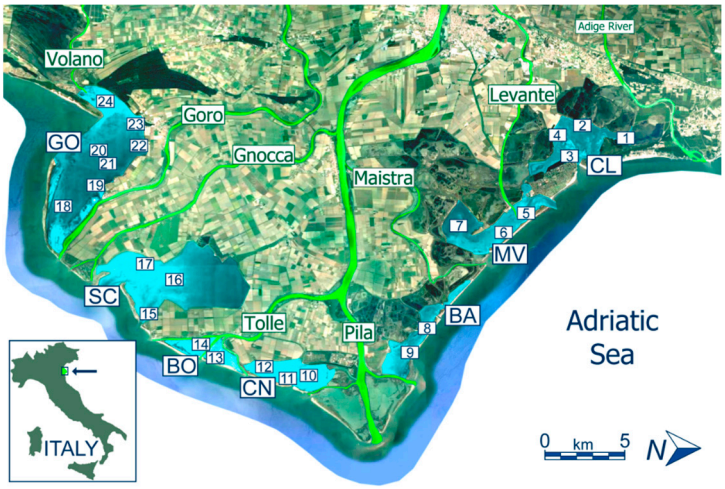

Figure 1. Map of the Po Delta, along with names of distributaries. Sampling sites are labelled with two capital letters identifying the lagoon and core numbers from 1 to 24: CL = Caleri, MV = Marinetta-Vallona, BA = Barbamarco, CN = Canarin, BO = Bonelli, SC = Scardovari, GO = Goro.

The investigated lagoons have diversified characteristics in terms of morphology, hydrodynamics, salinity, freshwater inputs and water exchanges with the coastal zone, although they belong to the same deltaic system. The average water depth varies from 0.9 m

(CN) to 1.8 m (MV). Comprehensive descriptions of the morphological, hydrological and naturalistic aspects of the lagoons [17]; water circulation, mean salinity and renewal times, based on the results of a hydrodynamic model [18]; and surface sediment characteristics and heavy metal contamination in the seven lagoons [16] have been reported.

2.2. CT-Scan Examination

Sediment cores were analysed by X-ray CT scan with a 1-mm down-core resolution using a Philips (Amsterdam, The Netherlands) MX8000 IDT 16 System (voltage = 120 kVp, scanning dose = 211–393 mA). Tomographic intensity profiles measured along the core (CT number, expressed in HU units on the Hounsfield scale) depend on the thickness of the sediment slab considered and the software setting (i.e., the intensity of the X-ray, as well as the algorithms used) [19]. Maximum (MIP) and minimum (MinIP) intensity projection algorithms, respectively, return the highest and the lowest attenuation values encountered in a given sediment volume, highlighting the presence of high- or low-density volumes. The average intensity projection (AIP) algorithm returns the average of each component attenuation value encountered.

Intrinsic inhomogeneity in the sediment layers, as well as the presence of high-density objects (e.g., shells, shell fragments and pebbles) or low-density structures (e.g., those due to the presence of voids, water/gas "bubbles" [20–22], worm burrows, remains of plant roots), contribute to uncertainties in the CT number (see Supplementary Materials).

To obtain a representative value and reduce the degree of uncertainty, the CT number was measured under AIP conditions in 20-mm-thick axial slices of the core, following the procedure described in Figure 2. This procedure was chosen for optimal comparison of the CT measurement with sediment features in 20-mm-thick subsamples passed through a 1-mm mesh for water content, organic matter and grain-size measurements.

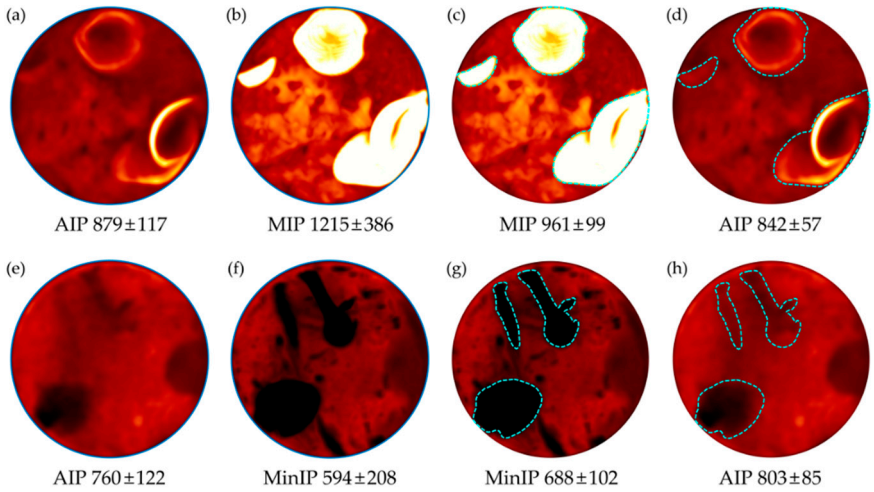

Figure 2. CT-scan images of a 20-mm-thick slab of sediment cores GO20 (**a**–**d**) and SC17 (**e**–**h**); the CT number ± standard deviation (STD) in HU units is shown below each image. (**a**) Average Intensity Projection (AIP) algorithm and (**b**) Maximum Intensity Projection (MIP) algorithm of the whole axial slice; (**c**) MIP algorithm with high-density regions of interests (ROI—white areas, contoured) removed; (**d**) AIP algorithm with high-density ROI removed from CT number calculation; (**e**) AIP algorithm and (**f**) Minimum Intensity Projection (MinIP) algorithm of the whole axial slice; (**g**) MinIP algorithm with low-density ROI (dark areas, contoured); (**h**) AIP algorithm with low-density ROI removed from CT number calculation.

High-density volumes (Figure 2a–d) were identified under MIP conditions as the region of interest (ROI), isolated with contours and then, using the ROI editing procedure, were discarded in the recalculation of the CT number under AIP conditions. A similar procedure was used under MinIP conditions to discard large low-density volumes (Figure 2e–h). Both kinds of ROIs were carefully observed before being excluded using

the 2D and 3D tools made available by the software. Unless otherwise stated, from here onwards, the term CT number is meant for measurements obtained under AIP conditions using the procedure illustrated in Figure 2.

The CT numbers measured in this manner were better correlated with the W_C of sediments than the CT numbers measured under MIP or MinIP algorithms. More details on the procedure are described in Supplementary Materials.

In each core, the procedure described above was applied to all the 2-cm-thick axial slices from which sediment aliquots were taken for the analyses described in Section 2.3. The final CT number was then compared with various features of the sediment subsample sieved through a 1-mm mesh. Obviously, after the core opening, free water and gases (from bubbles) were lost.

2.3. Core Subsampling and Sediment Analyses

The Plexiglas cylinders were split lengthwise, and one-half sediment cores were sampled by selecting 2-cm-thick layers at different depths along the profile; the top (0–10 cm) sections were continuously sampled, producing 5 samples, and the layers below were selected on the basis of CT images. Wet sediment samples were sieved through a 1-mm Teflon mesh to remove shells and other debris and thoroughly homogenised.

W_C was determined from an aliquot of a sample dried in an oven at 105 °C until it reached a constant weight [23]. Based on variation coefficients of 7 replicate measurements in 2 sediment samples, the analytical error of W_C determination was less than 0.65%.

Other variables were derived from W_C, following Hobbs' assumptions and formulas [24]. The assumptions were as follows: (i) The pore space in the sediment is completely water saturated (no gases); (ii) The density of pore water (ϱ_w) is 1.0 g cm^{-3}; (iii) The mean density of dry sediment particles (ϱ_p) is correctly estimated. As the terminology in soil and sediment studies is not uniform, we specify the definitions and the equations used in this study, as follows:

W_c is the weight fraction of water in the total weight of wet sediment,

$$W_c = W_w/(W_w + W_s), \quad (1)$$

where W_w denotes water weight and W_s means dry sediment weight.

For a unit weight of water sediment mix ($W_w + W_s = 1$), W_c in g equals W_w.

Porosity (Φ) is the volume fraction of water in the total volume of wet sediment,

$$\Phi = V_w/(V_w + V_s), \quad (2)$$

where V_w signifies water volume and V_s refers to dry sediment volume.

$$V_w = W_c/\varrho_w = W_c, \text{ as water density } \varrho_w = 1$$

$$V_s = W_s/\varrho_p = (1 - W_c)/\varrho_p,$$

where ϱ_p is the mean sediment particle density in g cm^{-3}; thus,

$$\Phi = W_{c/}(W_c + (1 - W_c)/\varrho_p) \quad (3)$$

Bulk density (ϱ_{bw}) is the weight of wet sediment in a unit volume (g cm^{-3})

$$\varrho_{bw} = (W_w + W_s)/(W_w + W_s/\varrho_p) = 1/(W_c + (1 - W_c)/\varrho_p) \quad (4)$$

or

$$\varrho_{bw} = \Phi/W_c$$

It should be noted that the bulk density used to match the values of the CT number was calculated from W_C in a fraction of sediment matrix after removing all larger shells

or shell fragments and other debris. More precisely, it was thus the bulk density of the sediment matrix rather than the bulk density of the total sediment.

The mean sediment particle density (ϱ_p) was estimated by assuming constant densities of mineral fraction (ϱ_m) and OM fraction (ϱ_o). Following Avnimelech et al. [25], we assumed the conversion factor of organic carbon (OC) to OM to be 1.7, and thus:

$$\varrho_p = (OM \times \varrho_o) + (100 - OM) \times \varrho_m)/100, \quad (5)$$

where OM = 1.7 × OC in %, and

ϱ_o = 1.25 and ϱ_m = 2.65 g cm^{-3} were assumed for the density of organic and mineral fraction, respectively [25].

W_C was not corrected for salt, as this correction is considered negligible ([26], cited after [24]). Based on the modelled mean surface water salinity on various sites in lagoons [18], we estimated that introducing a correction for salt would change the calculated bulk density value by a maximum of 0.33%.

Grain-size analysis was carried out on a wet aliquot sample of about 2 g, using a Mastersizer 2000 analyser (Mastersizer 2000, Malvern Instruments, Malvern, UK), which provided the volumetric percentages of particles within 100 contiguous dimension classes covering the 0.02–2000-µm range.

Total nitrogen (TN) and total carbon (TC) were determined on duplicate samples using a ThermoFisher Flash 2000 IRMS Elemental Analyzer (EA, ThermoFisher Scientific Inc., Aurora, OH, USA). Subsamples for OC measurements were first decarbonated with HCl 1.5 N. Determined by replicate analyses of the same sample, each measurement had an average standard deviation (STD) of ±0.07% for OC and ±0.009% for TN. Inorganic carbon (IC) was calculated as the difference between TC and OC.

About 0.4 g of the sample dried at 55 °C was digested with 8 mL of HNO_3 8N in a microwave oven [27], and after filtration, the iron (Fe) concentration was determined by Inductively Coupled Plasma—Atomic Emission Spectrometry (ICP-AES—Optima 2100DV, PerkinElmer, Waltham, MA, USA) [28]. Determined using six replicates of homogenised samples, the analytical precision was 6%. A certified reference material sample (PACS-2—Marine Sediment Reference Materials for Trace Metals and other Constituents, National Research Council of Canada) was digested and analysed five times in accordance with the sediment sample analysis procedure. The mean recovery was 75%, indicating that a part of Fe was bound to refractory minerals (e.g., alumina silicates and/or some resistant sulphides). The measured content of Fe is thus considered an extractable fraction. The calibration for ICP-AES analysis was achieved using external standards via the multiple-point curve approach. Full calibration was performed after each set of 48 samples.

The CT-scan data were processed with Horos v2.0.2 (Horos Project, Free DICOM Medical Image Viewer), an open-source code software distributed free of charge under the Lesser General Public License at Horosproject.org and sponsored by Nimble Co LLC d/b/a Purview in Annapolis, MD, USA.

Statistical calculations were performed using PAST 3.4 for Windows (University of Oslo, Oslo, Norway) and StatPlus for Mac (AnalystSoft Inc., Walnut, Canada).

3. Results and Discussion

3.1. Sediment Characteristics

The statistical data for the distribution of the relevant variables measured in the sediment samples are shown in Table 1. Distributions of water, fine particles (<16 µm) in the clay plus fine silt dimensional classes and OC percentages with sediment depth are shown in Figure 3.

Table 1. Statistical description of the relevant variables measured in the 252 sediment samples collected from the 24 cores. (1) calculated from water content (W_C) using Equations (3) and (4); (2) percentage of particles with diameter <16 µm; (3) Fe concentration extractable with 8N HNO_3; (4) coefficient of variation.

	W_C %	OC %	Porosity (1) %	Bulk Density (1) g cm^{-3}	TN %	<16 µm (2) %	IC %	Fe (3) %	CT Number HU
Minimum	18.4	0.18	37.4	1.28	0.016	5.2	1.13	1.3	491
Maximum	64.2	2.39	82.4	2.03	0.322	77.9	4.07	4.3	1389
Median	39.6	0.9	62.7	1.58	0.100	38.5	2.13	2.6	876
Mean	41.2	1.01	63.6	1.59	0.116	43.2	2.16	2.2	906
STD	11.2	0.46	10.7	0.18	0.060	17.4	0.43	0.6	229
CV% (4)	27.1	45.0	16.9	11.2	51.3	40.3	19.9	21.5	25.3

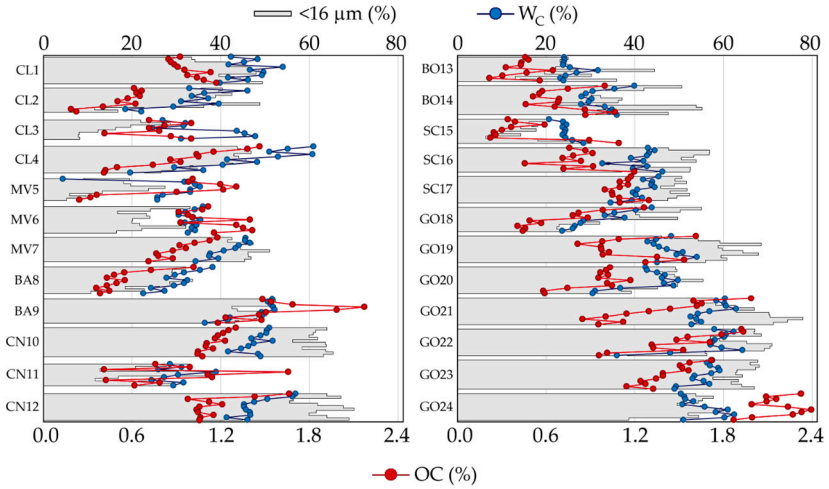

Figure 3. Percentages of water content, fine particles and organic carbon in the 252 sediment layers analysed in the 24 cores. For each core, the sequence of investigated layers with depth is shown from left to right.

Fine particle distribution depends on the hydrodynamic characteristics, sediment transport from the Po River distributaries and processes that occur along the coastline. A higher content of fine particles in the surface sediment layer (0–10 cm) is observed in the lagoons located south of the main distributary (Po di Pila), with the exception of the sites close to the tidal inlets (CN11, SC15) or near the river branch (BO13), where strong currents prevent their sedimentation [16]. On a few sites, sediments in the deeper part of the cores are depleted in fine fraction (e.g., CL3, MV5, GO18), suggesting more energetic hydrodynamics in the past.

OC content generally decreases with depth, but in some cores, clear minima or maxima are observed at intermediate depths, indicating modifications of the environmental setting or the sediment delivery.

It is worth pointing out that the set of 252 samples shows large ranges in the values of the main physico-chemical variables considered, as evidenced by the coefficient of variation in percent (CV%) values (Table 1), particularly for water, fine particles and TN and OC contents. Such a well-diversified set of sediment samples is suitable for the evaluation of the usefulness of the CT-scan investigation in reflecting sediment features prior to core opening.

3.2. CT Number, Bulk Density and Water Content

The mean CT numbers obtained from the selected volume of the examined slices, as shown in Figure 2 (Section 2.2), are compared with the matrix bulk density calculated from the measured W_C and the assumed density of sediment particles (Equations (4) and (5)). A relatively narrow range of mean particle densities (2.59–2.65 g cm^{-3}) is estimated from the

proportions of mineral and organic particles. The calculated matrix bulk density varies largely (1.3–2.0 g cm^{-3}) because of the considerable range of W_C.

In Figure 4, the CT numbers are plotted against the calculated bulk densities of 252 samples from 24 cores recovered from the 7 lagoons. For comparison, calibration fits obtained by other authors [29–31] who used various density standards and a similar setting of the CT scanner, particularly an X-ray energy of 120 keV, are also shown. Although the determination coefficient for our data is lower than those obtained for calibration fits using various standards, the differences in regression coefficients are minor (Table 2).

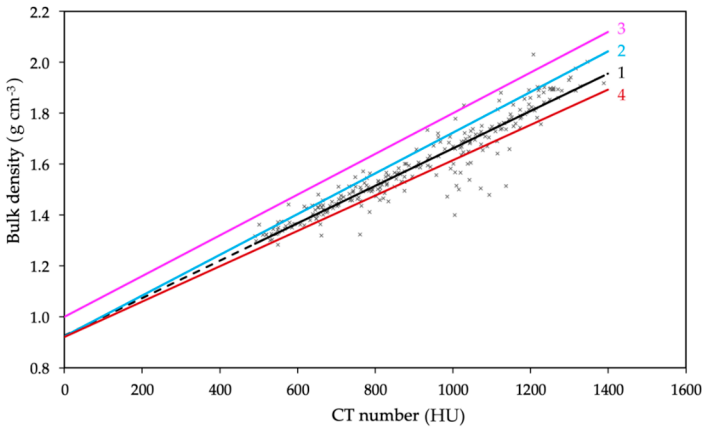

Figure 4. Relation between measured CT numbers obtained with Average Intensity Projection (AIP) on manually selected volumes (see Section 2.2) and calculated bulk density of sediment (crosses and black regression line no. 1). Lines 2–4 correspond to CT number calibration obtained by various authors using density standards (cf. Table 2).

Table 2. Statistics of regressions shown in Figure 4. Regressions 2–4 are obtained using various homogeneous and heterogeneous density standards, such as water, bentonites, wood and rocks. All CT numbers are obtained using X-ray energy of 120 keV.

Regression	Intercept	Constant	R^2	Reference
1	0.926	7.36×10^{-4}	0.893	this work
2	0.924	8.0×10^{-4}	0.990	[29]
3	1	8.0×10^{-4}	0.933	[30]
4	0.921	6.94×10^{-4}	0.992	[31]

Considering a large set of samples with broad ranges of W_C, sediment texture and some variations in chemical composition (Table 1), the fact that the calculated bulk density explains nearly 90% of the variability of the CT number is a quite satisfactory result, better than that reported in a study [32] from a lake sediment core using direct measurements of bulk density (R^2 = 0.59).

Although the methods for deriving the bulk density value from the CT number seem reliable, the underlying principles are not always well constrained for various types of sediments. Orsi et al. [1] studied shallow-water Louisiana shelf sediments and found a generally good correlation between the CT number and the bulk density, measured with a traditional method. They noticed occasional deviations from expected values, explained by the presence of shell fragments and gas bubbles, as well as imperfect adequacy between volumes measured with a CT scan and sampled for bulk density determinations. Consequently, the CT number value derived from the total volume of a sediment slab corresponds to a "true" bulk density, while the selective measurement that avoids the obvious heterogeneities due to shells or bubbles reflects a "matrix" density. The variability of the bulk density of recent, water-saturated sediments depends essentially on W_C, OM content and the mean density of the mineral phase. These parameters are strongly interrelated in soils and sediments [25,33,34].

As shown in Figure 5a, the CT number depends inversely and linearly on porosity (Φ), with the determination coefficient similar to the coefficient found for the CT number–bulk density relation. This is because porosity is calculated from the measured W_C and the estimated mean sediment particle density (ϱ_p), combining Equations (3) and (5). Although calculated porosity explains 89% of the CT number variability, other factors must significantly contribute to some data points' considerable deviations from the best fit. It is evident that the uncertainty of ϱp cannot explain these deviations, as shown by the blue and the red regression lines depicting the linear relations, assuming the mean specific density of sediment particles fixed at 2.5 and 2.8 g cm^{-3}, respectively. This range of the mean density of particles is likely valid for all samples examined in this study. Fortin et al. [32] reported a determination coefficient (R^2) of 0.83 for the linear regression CT number versus porosity (calculated from wet and dry bulk density), comparable to R^2 = 0.89 in this study. They observed that the correlation was weaker for lower porosity and attributed this tendency to the errors in the discrete sampling for bulk density measurements; in fact, these errors correspond to a percentage of the mass per cubic centimetre and hence they increase in denser samples.

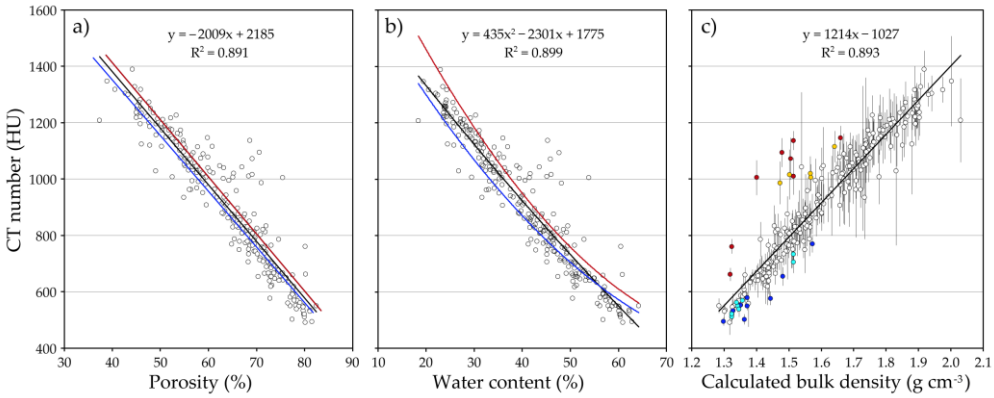

Figure 5. (**a**) Calculated porosity versus measured CT number with the linear regression (black line) explaining 89% of the CT number variability. Blue and red lines depict the linear relations, assuming constant sediment particles' specific densities of 2.5 and 2.8 g cm^{-3}, respectively. (**b**) Plot of measured water content against CT number. Polynomial (black line) and linear (not shown) fits to the data points are very similar. Blue and red lines show the expected relations between water content and CT number, calculated using Equation (4) with two particle densities of 2.5 and 2.8 g cm^{-3}, respectively, and coefficients resulting from CT versus bulk density regression (Figure 5c). (**c**) Calculated bulk density against CT number plotted as dependent variable. Error bars show 1 STD of the mean CT number measured on selected volumes, as described in Section 2.2. Samples with residuals larger than 3 STDs of CT number are filled with red and blue for positive and negative residuals, respectively. Samples with residuals larger than 2 STDs of CT number are filled with orange and light blue for positive and negative residuals, respectively.

At a W_C exceeding 40%, ϱ_p has very little influence on the CT number, but at a lower W_C, the importance of ϱ_p increases (Figure 5b). For example, at 60% W_C, the difference between the CT numbers calculated with ϱ_p of 2.5 and 2.8 is 40, while it is about 150 for 20% W_C. It should be noted that linear and polynomial fits to our experimental data are very similar. It might be that at a very high W_C, part of the water is lost during subsampling; thus, W_C is underestimated in these samples, increasing linearity.

A closer examination of the plot of the calculated matrix bulk density against the mean CT number (Figure 5c) reveals strong differences in STDs of the mean CT number and some distinct outliers. The STD increases with the heterogeneity of sediments. An inspection of residuals of the regression indicates that 32 out of the 252 (12.7%) samples deviate from the best fit by more than 2 STDs of the mean CT number. Among them, 17 (6.7%) samples deviate by more than 3 STDs. These samples are marked with different colours in Figure 5c.

Most probably, some deviations are due to poor correspondence between the measured mean CT number of the sediment matrix and the measured W_C. On one hand, the W_C is determined with a small aliquot of sediment. On the other hand, in some sediment layers with abundant shells or numerous low-density volumes, CT numbers are determined using only a part of the total layer volume. Another reason could be the underestimation of the W_C due to a loss of a fraction of water during subsampling, which may occur especially at a high W_C.

It is unlikely that strong deviations are due to variations in the mean sediment particle density, unless heavy minerals are strongly enriched in some grain-size classes. Such enrichment can occur due to size-density sorting [35], but no data on heavy minerals in the recent sediment from lagoons in the Po Delta are available.

It is interesting that the majority of the samples showing high positive residuals of regression (Figure 5c) are found in cores from the CL Lagoon. In contrast, most of the samples that have negative residuals are collected from the GO Lagoon. These two lagoons are situated at the northern and the southern extremities of the modern Po Delta (Figure 1), respectively, and have accumulated sediments of different origins and experienced different environmental conditions [16,18].

X-ray attenuation expressed as the CT number is sensitive not only to the Compton effect, which is related to bulk density, but also to the photoelectric effect, which increases with the atomic number (Z) of the elements present in sediments. Duchense et al. [36] demonstrated that the photoelectric effect increased for aragonite and calcite with respect to quartz, the minerals common in lagoon sediments. Orsi and Anderson [37] showed that CT numbers could be precisely calibrated in terms of the bulk density using an artificial mixture of SiO_2 and seawater, although they noticed a difference in calibration when using quartz or carbonates as sediment surrogates. This is because the photoelectric effect is more important for Ca (atomic number = 20) than for Si (atomic number = 14). However, at an X-ray energy of >100 keV, variations in the effective atomic numbers of sediments forming major elements have little impact on the CT number due to the small photoelectric effect [34]. The difference in CT numbers increases with decreasing W_C or increasing bulk density. For example, at bulk densities of 1.3 and 2.0 g cm^{-3}, the CT number for calcite compared with silica increases by 12% and 20%, respectively, at an X-ray energy of 120 kVp [38].

However, in our study, the samples showing positive residuals of regression (Figure 5c) higher than three STDs of the CT number, all from the CL Lagoon, have relatively elevated W_C (mean = 50%, range = 36–61%), corresponding to a mean bulk density of 1.6 g cm^{-3} (range = 1.4–1.8). In these samples, the measured CT numbers are 15–50% higher than those predicted from regression. Neither carbonates nor extractable Fe contents are significantly higher in these samples compared with the remaining samples from the CL Lagoon.

Consequently, it seems that Ca from carbonates or Fe oxides/sulphides are not responsible for the increased CT number. At present, the CL Lagoon is not directly connected to the Po River distributaries, but deltaic deposits in this region are alternatively alimented by the Po and the Adige Rivers. The composition of major elements of sediments carried by these two rivers is not distinct enough to provide a fingerprint of provenance [39]. More detailed studies would be necessary to confirm and possibly explain the observed deviations, but some hints can be obtained from the available data (Sections 3.3 and 3.4).

3.3. Relations between Water Content and Sediment Characteristics

The W_C of sediments is well correlated with the percentage of fine silt and clay fractions (<16 μm), with OC and TN contents. The regressions of W_C against these variables are shown in Figure 6a, and the corresponding statistics are listed in Table 3. Generally, fine-grained and organic-rich unconsolidated sediments retain more water than sandy and organic-poor sediments (e.g. [25]). A comprehensive discussion of the relations between bulk density, W_C and sediment composition in surface shelf and lagoon sediments is presented by Flemming and Delafontaine [40]. The higher determination coefficient for

the regression of W_C against TN as compared with OC can probably be explained by concomitant preferential nitrogen mineralisation of OM and sediment compaction with depth. The linearity of the relations between W_C and both TN or OC seems lost for the highest values of independent variables (Figure 6a); thus, second-degree polynomial fits represent these relations better (Table 3). It seems that when TN and OC contents exceed 0.2 and 1.8%, respectively, water saturation capacity is reached. On the contrary, the relation between WC and <16-µm fraction remains linear for the full range of measured values.

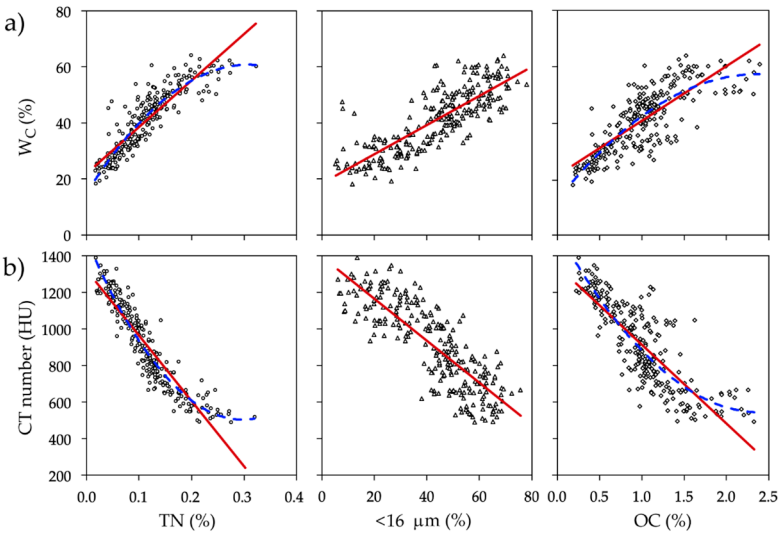

Figure 6. Contents of total nitrogen (TN), <16-µm grain-size fraction (<16 µm) and organic carbon (OC) plotted against (**a**) water content and (**b**) CT number. Linear regression (solid lines), and for TN and OC, second-degree polynomial fit (broken line) correspond to regression coefficients shown in Table 3.

Stepwise multiple linear regression of W_C against the percentage of TN and <16-µm fraction explains 84% of W_C variability (Figure 7a), whereas an addition of OC as the third variable does not improve R^2 adj. anymore (Table 3). In 10 out of the 252 samples, measured values are higher than predicted values by more than 20%, all from the cores collected in the CL Lagoon. Among these 10 samples, 8 also show over 20% deviations from the best fit of the CT number versus bulk density (Figure 5c).

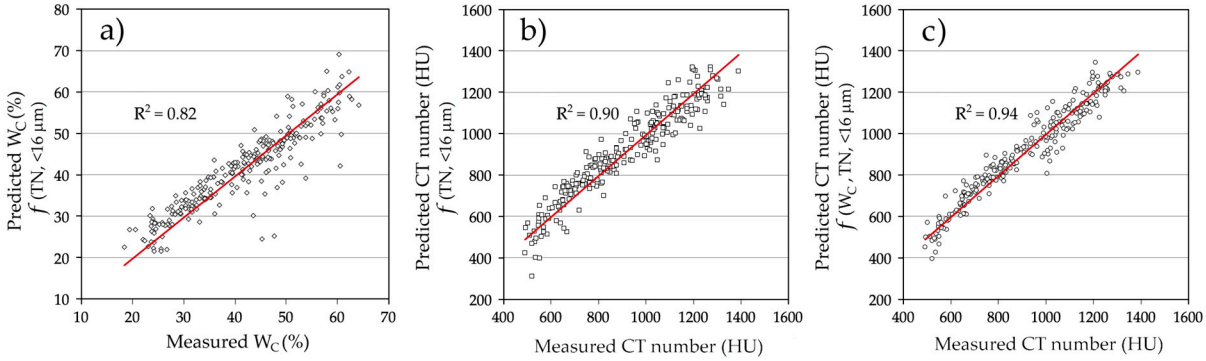

Figure 7. Plots of measured versus predicted values with multiple linear regression models. Variables used in regression models (**a**), (**b**) and (**c**) are indicated on *y*-axis. R^2 is the determination coefficient of linear fit forced to pass through origin. Model parameters are shown in Table 3.

Table 3. Regression statistics for water content and CT number as dependent variables. * number of samples; it is 252 when not reported.

		Dependent Variable: W_C Independent Variables			Dependent Variable: CT Number Independent Variables			
Regression Type		**TN**	**<16 µm**	**OC**	**W_C**	**TN**	**<16 µm**	**OC**
linear	R^2	0.79	0.66	0.63		0.85	0.70	0.67
	x coefficient	166	0.52	19.3		−3527	−11	−410
	intercept	22	19	22		1316	1384	1323
polynomial	R^2	0.83		0.67		0.90		0.71
	x^2 coefficient	−481		−7.95		10,876		155
	x coefficient	279		38		−6500		−769
	intercept	15		13		1476		1494
linear partial	limit	<0.2%		<1.8%		<0.2%		<1.8%
	R^2	0.79		0.64		0.87		0.68
	x coefficient	202		23.4		−4344		−492
	intercept	19		18		1389		1390
	n *	227		236		227		236
Multiple reg. 1	R^2 adj.	0.84				0.90		
	x coefficient	118	0.22			−2629	−4.6	
	intercept	17.7				1403		
Multiple reg. 2	R^2 adj.	0.84				0.90		
	x coefficient	120	0.22	−0.21		−2629	−4.6	10.9
	intercept	17.8				1400		
Multiple reg. 3	R^2 adj.	0.93						
	x coefficient	−12.6	−1432					
	intercept	1593						
Multiple reg. 4	R^2 adj.	0.94						
	x coefficient	−9.7	−1394	−2.46				
	intercept	1575						
Multiple reg. 5	R^2 adj.	0.94						
	x coefficient	−9.7	−1466	−2.42	8.9			
	intercept	1572						

3.4. Relations between CT Number and Sediment Characteristics

Boespflug et al. [41] used CT number profiles for the detection of lamination in St. Laurence estuary sediments and observed an inverse correlation of the CT number with sediment grain size and OM measured in light and dark laminae. As these variables control the W_C of sediments, the relations were probably indirect.

Here, the relations between the CT number and the sediments' TN, OC and <16-µm fraction are tested by simple (Figure 6b) and stepwise multiple regressions (Figure 7b,c and Table 3). These relations are similar to those for W_C, but all determination coefficients are higher. Multiple linear regression with just two independent variables (TN and <16-µm fraction) explains 90% of the variability of the CT number compared with 84% for W_C (Table 3). Moreover, none of the 10 samples from the CL Lagoon cores showing more than 20% deviations from predicted values in W_C multiple regression (Figure 7a) against the same independent variables strongly deviates from predicted CT number values (Figure 7b). This suggests that W_C values, rather than CT number measurements, are not representative for these samples.

Although the reason for inadequate W_C values is not clear, it should be noted that some CL Lagoon samples show considerable heterogeneity due to their high content of shell fragments, and possibly measured CT number values reflect true W_C better than direct measurements in a small subsample. Five samples show higher measured CT number values than the predicted ones by more than 20%. These samples, all from the top layers

of three GO Lagoon cores, have TN contents among the highest measured (0.23–0.32%). At these contents, the relations between the CT number or W_C and TN lose their linearity (Figure 6). When W_C is added to the independent variables, this problem is partly corrected, increasing the R^2 adj. to 0.94 (multiple regression 4 in Table 3 and Figure 7c).

4. Conclusions

Various software algorithms available for the CT-scan investigation of sediment cores have been explored to optimise conditions for the observation of sediment structure along vertical profiles and the visualisation of high-density objects (Maximal Intensity Projection) or low-density volumes (Minimal Intensity Projection). CT numbers obtained with Average Intensity Projection reflect the bulk density of the sediment matrix throughout the lagoons of the Po Delta, and the segmentation procedure with the selection of regions of interest reduces measurement uncertainty.

The water content of sediments and the CT number are well correlated. Multiple linear regression shows that two variables, total nitrogen and <16-μm fraction, explain 90% of the CT number variability.

The measurement of the CT number prior to core opening provides not only a proxy of sediment water content but also an indirect estimation of fine fraction and organic matter (organic carbon and total nitrogen) contents.

Supplementary Materials: The following are available online at https://www.mdpi.com/2077-1312/9/3/323/s1, Figure S1: CT number profiles measured in a sagittal slice of core MV7, with five different algorithms and two thicknesses of the investigated slice, and the corresponding CT images of the core; the measurement axis is superimposed; Figure S2: CT number profiles measured in five sagittal slices (a–e) of core MV7 in AIP (6.2) conditions; Figure S3: (a) Detail of CT image of core MV7 and position of profile <e> shown in Figure S2, where it intersects a low-density volume; (b) CT number values measured along a segment of profile <e>; (c) axial CT image of the same low-density volume. Both CT images obtained under AIP (6.2) conditions; Figure S4: (a) Detail of CT image at depths close to the base of core MV7 (around 554-mm depth) and position of the stroke of profile <f> where (b) CT number is measured in MIP (13.2) conditions. Three-dimensional rendering of (c) sagittal and (d) axial sections; Figure S5: Regressions for CT number obtained with MIP, AIP and MinIP settings with respect to water content (WC), organic carbon (OC), fine particle content (<16 μm) and total nitrogen (TN).

Author Contributions: Conceptualization, J.D., G.F. and R.Z.; methodology, D.C. and R.Z.; validation, J.D., G.F. and R.Z.; formal analysis, J.D., G.F. and R.Z.; investigation, J.D., G.F. and R.Z.; resources, D.C. and R.Z.; data curation, D.C. and R.Z.; writing—original draft preparation, J.D. and R.Z.; visualization, R.Z.; project administration, R.Z.; funding acquisition, R.Z. All authors have read and agreed to the published version of the manuscript.

Funding: This research was financed by the National Flagship Project RITMARE ("The Italian Research for the Sea"), coordinated by the Italian National Research Council and funded by the Italian Ministry of Education, University and Research.

Data Availability Statement: The data presented in this study are available on request from the corresponding author. The data are not yet publicly available but will be published soon.

Acknowledgments: The authors thank Margherita Botter, Gianfranco Magris and Andrea Pesce (CNR ISMAR, Venice, Italy) for their assistance in sampling and analyses, Roberto Pini (CNR IRET, Pisa, Italy) for the grain-size analysis, Leonardo Langone and Fabio Savelli (CNR ISMAR, Bologna, Italy) for the elementary analyses, and Luca Ghezzo for CT-scan analyses at the San Camillo Hospital (Venice, Italy).

Conflicts of Interest: The authors declare no conflict of interest.

References

1. Orsi, T.H.; Edwards, C.M.; Anderson, A.L. X-Ray computed-tomography—A non-destructive method for quantitative analysis of sediment cores. *J. Sediment. Res. Sect. A Sediment. Petrol. Process.* **1994**, *64*, 690–693. [CrossRef]
2. Cnudde, V.; Boone, M.N. High-resolution X-ray computed tomography in geosciences: A review of the current technology and applications. *Earth-Sci. Rev.* **2013**, *123*, 1–17. [CrossRef]
3. St-Onge, G.; Long, B.F. CAT-scan analysis of sedimentary sequences: An ultrahigh-resolution paleoclimatic tool. *Eng. Geol.* **2009**, *103*, 127–133. [CrossRef]
4. Reilly, B.T.; Stoner, J.S.; Wiest, J. SedCT: MATLAB tools for standardized and quantitative processing of sediment core computed tomography (CT) data collected using a medical CT scanner. *Geochem. Geophys. Geosyst.* **2017**, *18*, 3231–3240. [CrossRef]
5. Dorador, J.; Rodriguez-Tovar, F.J. High-resolution image treatment in ichnological core analysis: Initial steps, advances and prospects. *Earth-Sci. Rev.* **2018**, *177*, 226–237. [CrossRef]
6. Ma, S.H.; Zheng, J.N.; Tang, D.W.; Li, Y.P.; Li, Q.P.; Lv, X. Application of X-Ray Computed Tomography Technology in Gas Hydrate. *Energy Technol.* **2019**, *7*. [CrossRef]
7. Duck, Y.; Lorke, A.; Jokiel, C.; Gierse, J. Laboratory and field investigations on freeze and gravity core sampling and assessment of coring disturbances with implications on gas bubble characterization. *Limnol. Oceanogr. Methods* **2019**, *17*, 585–606. [CrossRef]
8. Tonai, S.; Kubo, Y.; Tsang, M.Y.; Bowden, S.; Ide, K.; Hirose, T.; Kamiya, N.; Yamamoto, Y.; Yang, K.H.; Yamada, Y.; et al. A New Method for Quality Control of Geological Cores by X-Ray Computed Tomography: Application in IODP Expedition 370. *Front. Earth Sci.* **2019**, *7*, 117. [CrossRef]
9. Nichols, M.M.; Boon, J.D. Sediment transport processes in coastal lagoons. In *Coastal Lagoon Processes (Elsevier Oceanography Series, 60)*; Kjerfve, E., Ed.; Elsevier Sciences Publishers: Amsterdam, The Netherlands, 1994; Volume 60, pp. 157–219.
10. Machado, A.S.; Dal Bó, P.F.F.; Lima, I.; Borghi, L.; Lopes, R. X-ray microtomography characterization of carbonate microbialites from a hypersaline coastal lagoon in the Rio de Janeiro State—Brazil. *Nucl. Instrum. Methods Phys. Res. Sect. A Accel. Spectrometers Detect. Assoc. Equip.* **2015**, *784*, 574–580. [CrossRef]
11. Amos, C.L.; Bergamasco, A.; Umgiesser, G.; Cappucci, S.; Cloutier, D.; DeNat, L.; Flindt, M.; Bonardi, M.; Cristante, S. The stability of tidal flats in Venice Lagoon—the results of in-situ measurements using two benthic, annular flumes. *J. Mar. Syst.* **2004**, *51*, 211–241. [CrossRef]
12. Emmanouilidis, A.; Messaris, G.; Ntzanis, E.; Zampakis, P.; Prevedouros, I.; Bassukas, D.A.; Avramidis, P. CT scanning, X-ray fluorescence: Non-destructive techniques for the identification of sedimentary facies and structures. *Revue Micropaléontol.* **2020**, *67*, 100410. [CrossRef]
13. Istituto Superiore per la Protezione e la Ricerca Ambientale—Gli Annali Idrologici. Available online: https://www.isprambiente.gov.it/it/progetti/cartella-progetti-in-corso/acque-interne-e-marino-costiere-1/progetto-annali/gli-annali-idrologici (accessed on 10 February 2021). (In Italian)
14. Pirrone, N.; Trombino, G.; Cinnirella, S.; Algieri, A.; Bendoricchio, G.; Palmeri, L. The Driver-Pressure-State-Impact-Response (DPSIR) approach for integrated catchment-coastal zone management: Preliminary application to the Po catchment—Adriatic Sea coastal zone system. *Reg. Environ. Chang.* **2005**, *5*, 111–137. [CrossRef]
15. Abbiati, M.; Mistri, M.; Bartoli, M.; Ceccherelli, V.U.; Colangelo, M.A.; Ferrari, C.R.; Giordani, G.; Munari, C.; Nizzoli, D.; Ponti, M.; et al. Trade-off between conservation and exploitation of the transitional water ecosystems of the northern Adriatic Sea. *Chem. Ecol.* **2010**, *26*, 105–119. [CrossRef]
16. Zonta, R.; Cassin, D.; Pini, R.; Dominik, J. Assessment of heavy metal and As contamination in the surface sediments of Po delta lagoons (Italy). *Estuar. Coast. Shelf Sci.* **2019**, *225*, 106235. [CrossRef]
17. Verza, E.; Cattozzo, L. *Atlante Lagunare Costiero del Delta del Po*; Regione del Veneto, Associazione Culturale Naturalistica Sagittaria, Consorzio di Bonifica Delta del Po: Taglio di Po-Rovigo, Italy, 2015; pp. 1–341. (In Italian)
18. Maicu, F.; De Pascalis, F.; Ferrarin, C.; Umgiesser, G. Hydrodynamics of the Po river-delta-sea system. *J. Geophys. Res. Oceans* **2018**, *123*, 6349–6372. [CrossRef]
19. Dalrymple, N.C.; Srinivasa, R.P.; Freckleton, M.W.; Chintapalli, K.N. Introduction to the Language of Three-dimensional Imaging with Multidetector CT. *RadioGraphics* **2005**, *25*, 1409–1428. [CrossRef]
20. Boudreau, B.P.; Algar, C.; Johnson, B.D.; Croudace, I.W.; Reed, A.; Furukawa, Y.; Dorgan, K.M.; Jumars, P.A.; Grader, A.S.; Gardiner, B.S. Bubble growth and rise in soft sediments. *Geology* **2005**, *33*, 517–520. [CrossRef]
21. Liu, L.; De Kock, T.; Wilkinson, J.; Cnudde, V.; Xiao, S.; Buchmann, C.; Uteau, D.; Peth, S.; Lorke, A. Methane Bubble Growth and Migration in Aquatic Sediments Observed by X-ray μCT. *Environ. Sci. Technol.* **2018**, *52*, 2007–2015. [CrossRef]
22. Zonta, R.; Cassin, D.; Pini, R.; Dominik, J. Substantial Decrease in Contaminant Concentrations in the Sediments of the Venice (Italy) Canal Network in the Last Two Decades—Implications for Sediment Management. *Water* **2020**, *12*, 1965. [CrossRef]
23. Percival, J.B.; Lindsay, P.J. Measurement of physical properties of sediments. In *Manual of Physico-Chemical Analysis of Aquatic Sediments*; Mudrock, A., Azcue, J.M., Mudrock, P., Eds.; CRC Press: Boca Raton, FL, USA, 1997; pp. 7–45.
24. Hobbs, C.H. A method for determining the dry bulk density of subaqueous sediments. *J. Sediment. Res.* **1983**, *53*, 663–665. [CrossRef]
25. Avnimelech, Y.; Ritvo, G.; Meijer, L.E.; Kochba, M. Water content, organic carbon and dry bulk density in flooded sediments. *Aquac. Eng.* **2001**, *25*, 25–33. [CrossRef]

26. Hamilton, E.L. Sound velocity and related properties of marine sediments, North Pacific. *J. Geophys. Res.* **1970**, *75*, 4423–4446. [CrossRef]
27. United States Environmental Protection Agency. *Method 3051A (SW-846): Microwave Assisted Acid Digestion of Sediments, Sludges, and Oils, Revision 1*; United States Environmental Protection Agency: Washington, DC, USA, 2007; pp. 1–30.
28. United States Environmental Protection Agency. *Method 2007: Determination of Metals and Trace Elements in Water and Wastes by Inductively Coupled Plasma-Atomic Emission Spectrometry, Revision 4.4*; United States Environmental Protection Agency: Cincinnati, OH, USA, 1994; pp. 1–58.
29. Gupta, L.P.; Tanikawa, W.; Hamada, Y.; Hirose, T.; Ahagon, N.; Sugihara, T.; Abe, N.; Nomura, S.; Masaki, Y.; Wu, H.Y.; et al. Examination of gas hydrate-bearing deep ocean sediments by X-ray Computed Tomography and verification of physical property measurements of sediments. *Mar. Pet. Geol.* **2019**, *108*, 239–248. [CrossRef]
30. Ashi, J. CT scan analysis of sediments from Leg 146. *Proceed. Ocean Drill. Program. Sci. Results* **1995**, *146*, 191–199.
31. Amos, C.L.; Sutherland, T.F.; Radzijewski, B.; Doucette, M. A rapid technique to determine bulk density of fine-grained sediments by X-ray computed tomography. *J. Sediment. Res.* **1996**, *66*, 1023–1039. [CrossRef]
32. Fortin, D.; Francus, P.; Gebhardt, A.C.; Hahn, A.; Kliem, P.; Lisé-Pronovost, A.; The PASADO Science Team. Destructive and non-destructive density determination: Method comparison and evaluation from the Laguna Potrok Aike sedimentary record. *Quat. Sci. Rev.* **2013**, *71*, 147–153. [CrossRef]
33. Gupta, S.C.; Larson, W.E. Estimating soil-water retention characteristics from particle-size distribution, organic- matter percent, and bulk density. *Water Resour. Res.* **1979**, *15*, 1633–1635. [CrossRef]
34. Keller, G.H. Organic matter and geotechnical proprieties of submarine sediments. *Geo-Mar. Lett.* **1982**, *2*, 191–198. [CrossRef]
35. Garzanti, E.; Andò, S.; Vezzoli, G. Settling equivalence of detrital minerals and grain-size dependence of sediment composition. *Earth Planet. Sci. Lett.* **2008**, *273*, 138–151. [CrossRef]
36. Duchesne, M.J.; Moore, F.; Long, B.F.; Labrie, J. A rapid method for converting medical Computed Tomography scanner topogram attenuation scale to Hounsfield Unit scale and to obtain relative density values. *Eng. Geol.* **2009**, *103*, 100–105. [CrossRef]
37. Orsi, T.H.; Anderson, A.L. Bulk density calibration for X-ray tomographic analyses of marine sediments. *Geo-Mar. Lett.* **1999**, *19*, 270–274. [CrossRef]
38. Akin, S.; Kovscek, A.R. Computed tomography in petroleum engineering research. *Geol. Soc. Lond. Spec. Publ.* **2003**, *215*, 23–38. [CrossRef]
39. Natali, C.; Bianchini, G. Geochemical proxies of sediment provenance in alluvial plains with interfering fluvial systems: A study case from NE Italy. *Catena* **2017**, *157*, 67–74. [CrossRef]
40. Flemming, B.W.; Delafontaine, M.T. Mass physical properties of muddy intertidal sediments: Some applications, misapplications and non-applications. *Cont. Shelf Res.* **2000**, *20*, 1179–1197. [CrossRef]
41. Boespflug, X.; Long, B.F.N.; Occhietti, S. CAT-scan in marine stratigraphy—A quantitative approach. *Mar. Geol.* **1995**, *122*, 281–301. [CrossRef]